Solid State Communications 253 (2017) 24–30

Contents lists available at ScienceDirect

Solid State Communications

journal homepage: www.elsevier.com/locate/ssc

Communication

Relaxation dynamics and thermodynamic properties of glassy $Tb_{0.5}Sr_{0.5}MnO_3$ single crystal

Hariharan Nhalil*, Suja Elizabeth

Department of Physics, Indian Institute of Science, Bangalore 560012, India

ARTICLE INFO

Keywords:
Single crystal
Spin-glass
Memory effect

ABSTRACT

Single crystals of $Tb_{0.5}Sr_{0.5}MnO_3$ were grown in an optical float zone furnace and their magnetic and thermodynamic properties were studied. Temperature dependent DC magnetization measurements at different fields show strong irreversibility below the magnetic anomaly at 44 K. The upward deviation from ideal CW behavior well above the transition temperature and its field independent nature are signatures of non-Griffiths phase. The origin non-Griffiths phase owe to competition between the antiferromagnetic and ferromagnetic Mn^{3+}–Mn^{4+} interactions mediated through intervening oxygen. Further, 44 K transition is confirmed as a magnetic glassy transition. The estimated dynamical spin flip time (τ_0=2.11(3)×10^{-14} s) and zv(9.3(2)) values fall into the range of typical spin-glass systems. Detailed memory and temperature cycling relaxation measurements were performed and support the Hierarchical relaxation model. Low-temperature specific heat data displays a linear term, identifying the glassy magnetic phase contribution.

1. Introduction

Doped rare earth manganites having general formula $R_{1-x}A_x$ MnO_3 (R=rare earth, A=Ca, Ba, Sr) have been known to possess interesting magnetic and physical properties such as metal–insulator transition, magnetoresistance and charge ordering [1–3]. Generally, the terminal members (x=0 and x=1) are antiferromagnetic and insulating in nature. By replacing the rare earth ion (R^{3+}) with divalent cation (A^{2+}), one can generate multiple valencies for the Mn ion which, in turn, results in ferromagnetic (FM) double exchange interaction and antiferromagnetic (AFM) superexchange interaction between Mn^{3+} and Mn^{4+} ions [4,5]. The chemical pressure due to size mismatch and multiple valencies (Mn^{3+}/Mn^{4+}) can modify the Mn–O bond length and Mn–O–Mn bond angle, which causes structural distortion [6]. The magnetic phase in these compounds is primarily controlled by the amount of hole doping (x), the average radius ($\langle r_A \rangle$) of A-site cations and the variance (σ^2) that determines the disorder due to random distribution of cations at the A site [7,8]. However, σ^2 and $\langle r_A \rangle$ have conflicting influence in determining the magnetic and transport properties [9]. For low value of σ^2, ferromagnetic metallic (FMM) state is preferred. As σ^2 increases, charge ordered antiferromagnetic (CO-AFM) state is commonly stabilized [9]. Any further increase in σ^2 results in an insulating spin-glass state [10]. If one analyzes $\langle r_A \rangle$ dependence, especially for its large values, the FMM state is favored [11]. As $\langle r_A \rangle$ decreases, FMM state transforms into CO-AFM, eventually reverting to an insulating spin-glass state as in $Nd_{0.5}Sr_{0.5}MnO_3$ ($\langle r_A \rangle$ = 1.236 Å) and $Y_{0.5}Ca_{0.5}MnO_3$ ($\langle r_A \rangle$ = 1.13 Å) [11,12]. The impact of cationic size ($\langle r_A \rangle$) is significant in charge ordering of manganites [7]. When $\langle r_A \rangle$ is small (<1.17 Å), the charge ordered state is robust and not sensitive to the magnetic field [7].

The parent compound $TbMnO_3$ is a well-known type II multiferroic material [20]. It shows three magnetic transitions, each at 8 K, 27 K and 42 K. Below 27 K, the system is multiferroic. The choice of Sr as dopant at trivalent Tb site stems from the option of using a divalent cation of larger ionic radius and the prospect of exploring the extent of structural distortion and magnetic phases in $Tb_{0.5}Sr_{0.5}MnO_3$ (TSMO50) [13,14]. Here, single crystal growth and magnetic and thermal properties of $Tb_{0.5}Sr_{0.5}MnO_3$ crystals are discussed in detail.

2. Experiment

Single crystals of $Tb_{0.5}Sr_{0.5}MnO_3$ were grown by float zone technique using optical four mirror image furnace. Single crystallinity of the grown crystal was confirmed through X-ray Laue diffraction and phase purity was established by powder XRD patterns of crushed single crystal using a Philips X'pert X-ray diffractometer and Cu K-α radiation. DC magnetization data was obtained in a Magnetic Property Measurement System (Quantum Design Inc.). AC susceptibility studies were carried out under 170 mOe field and at four different frequencies between 9 Hz and 1000 Hz. Specific heat measurements were per-

* Corresponding author.
E-mail addresses: hariharan@physics.iisc.ernet.in, hariharan.nhalil@gmail.com (H. Nhalil).

http://dx.doi.org/10.1016/j.ssc.2017.01.026
Received 4 October 2016; Received in revised form 6 January 2017; Accepted 29 January 2017
Available online 31 January 2017
0038-1098/

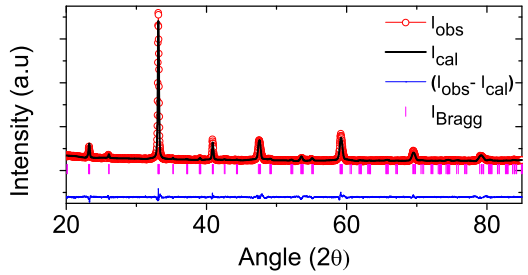

Fig. 1. (Color online) Powder XRD pattern of TSMO50 at room temperature. Rietveld refinement fit, difference pattern and Bragg positions are shown.

formed between 2 K and 300 K at 0 and 5 T fields.

3. Results and discussion

3.1. Structure

Powder XRD data of the crushed single crystal shows no trace of impurities within the detection limit of the instrument. Data was refined by Rietveld [15] method in orthorhombic *Pnma* space group (space group no.=62) utilizing FULLPROF suite [16]. XRD pattern along with the refinement results is shown in Fig. 1. Refined lattice constants in *Pnma* settings are a=5.4023(7) Å, b=7.6641(2) Å, and c=5.3963(3) Å. These satisfy $a \geq c \geq b/\sqrt{2}$ for O' type orthorhombic perovskite structure [17]. Detailed structural parameters are given in Table 1.

3.2. XPS

In order to analyze the changes in Mn valency with Sr^{2+} doping, XPS data was analyzed. The Mn 2p spectra of TSMO50 are presented in Fig. 2 along with Gaussian fits assuming the presence of both Mn^{3+} and Mn^{4+}. The binding energies (BE) obtained from the analysis were 653.66 eV (Mn $2p_{1/2}$) and 641.92 (Mn $2p_{3/2}$). A faithful fit of the observed $2p_{3/2}$ peak was obtained only by assuming mixed-valence for Mn. The peak positions of $2p_{3/2}$ are compared with MnO_2 and Mn_2O_3 where Mn ion is in 4+ and 3+ valence states, respectively. The $2p_{3/2}$ peak corresponding to MnO_2 is observed at 642.6 eV (Mn^{4+}), on the other hand, for Mn_2O_3, this peak is observed at 641.6 eV (Mn^{3+}). In the present case, corresponding peaks are observed at 643.38 and 641.56 eV, close to the reported values of Mn^{4+} and Mn^{3+}. This suggests that in our case Mn is present in both 3+ and 4+ ionic states. An estimate of the ratio of Mn^{4+} and Mn^{3+} from the area under the Gaussian fitted curves is 0.97 which is close to the expected ratio 1 suggesting that approximately equal amount of Mn^{4+} and Mn^{3+} ions are present in TSMO50.

Table 1
Refined lattice parameters, bond angles, bond lengths and refinement fit agreement factor derived from the room temperature XRD data.

Space group	Pnma
a	5.4023(7) Å
b	7.6641(2) Å
c	5.3963(3) Å
Volume	223.427(1) Å^3
$\langle$Mn–O–Mn$\rangle_{Avr}$	174.77(3)°
$\langle$Mn–O$\rangle_{Avr}$	1.837(4) Å
χ^2	1.96
Tolerance factor (t)	0.9259(2)
σ^2	0.0121
$\langle r_A \rangle$	1.20 Å

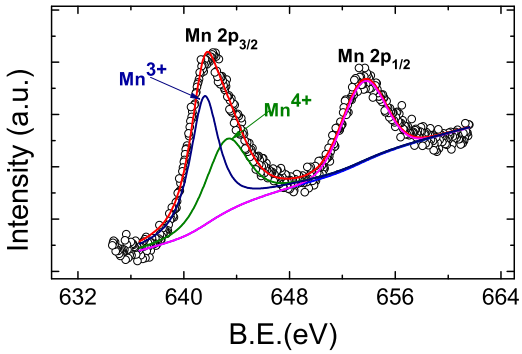

Fig. 2. (Color online) Mn 2p level XPS spectra of TSMO50. The graph also displays the Gaussian fitted curves assuming the presence of both Mn^{4+} and Mn^{3+}.

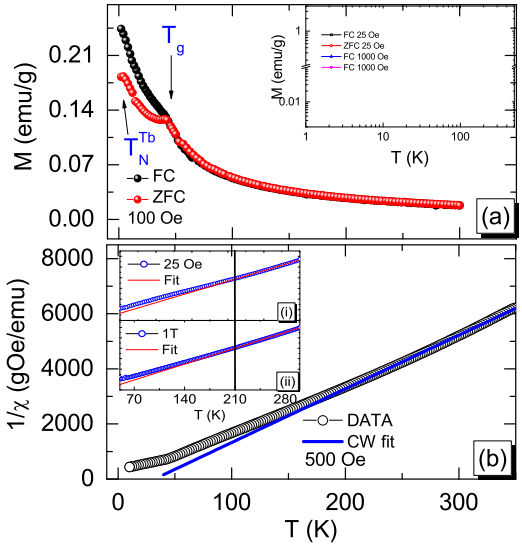

Fig. 3. (Color online) (a) Temperature dependent DC magnetization data at 100 Oe. The inset has plots at 25 Oe and 1000 Oe fields in log scale which show the decrease in bifurcation between FC and ZFC curves as the field increases. (b) Curie–Weiss fit in 230–350 K temperature range at 500 Oe. The inset shows the Curie–Weiss fit in the temperature range 230–300 K at (i) 25 Oe and (ii) 1 T fields.

3.3. DC and AC magnetization

FC/ZFC magnetization plots at 100 Oe field are illustrated in Fig. 3(a). The inset shows the plots at 25 Oe and 1000 Oe in log scale. At all three fields, the FC and ZFC curves display a clear hump-like feature at 44 K and bifurcate just below 44 K. The irreversibility in the FC/ZFC data below a threshold temperature is likely due to the presence of a spin-glass state [18]. As shown in the inset of Fig. 3(a), the extent of bifurcation decreases as the field increases. This is seen in half doped manganites which show spin-glass magnetic properties [19]. Below 44 K, both FC and ZFC curves show a steady rise. A possible explanation for this behavior is the high paramagnetic response of Tb^{3+} (9.72 μ_B) moments. AFM ordering of Tb ions is reflected as a broad peak at 8 K in ZFC plot (marked as a T_N^{Tb} in Fig. 3(a)) [20].

The inverse susceptibility ($1/\chi$) vs T plot at 500 Oe along with Curie–Weiss (CW) fit is illustrated in the main panel of Fig. 3(b). Curve fitting is done in the temperature range 230–350 K. The $1/\chi$ plot deviates from a straight line below ~230 K suggesting onset of magnetic ordering of Mn moments. The effective magnetic moment and CW temperature calculated from the fit are $\mu_{eff\,(E)}$ = 7.75 ± 0.06 μ_B/f. u. and θ=42.39(5) K, respectively. A positive value of θ is suggestive of dominant FM double exchange interaction over AFM superexchange interaction between Mn ions. Yoshii et al. [21] have observed similar behavior in polycrystalline TSMO50 but the